Neutron energy spectra from the laser-induced D$(d,n)^3$He reaction

D. Hilscher,[1,*] O. Berndt,[2] M. Enke,[1] U. Jahnke,[1] P. V. Nickles,[2] H. Ruhl,[2] and W. Sandner[2]
[1]*Hahn-Meitner-Institut Berlin, Glienickerstrasse 100, D-14109 Berlin, Germany*
[2]*Max-Born-Institut, Max-Born-Strasse 2A, D-12489 Berlin, Germany*

(Received 12 September 2000; revised manuscript received 11 January 2001; published 26 June 2001)

Detailed neutron energy spectra were measured for the D$(d,n)^3$He reaction induced in solid $(CD_2)_n$ targets by irradiation with 50-fs 2×10^{18} W/cm^2 light pulses from a 10-TW Ti:Sapphire laser. The neutrons were observed at two angles 5° and 112° relative to the incident laser beam. The neutron spectra at the two angles are characterized by peaks with large widths of about 700 keV full width at half maximum and a shift of 300 keV between them. Neutron energies of up to about 4 MeV were observed indicating that deuterons are accelerated up to an energy of 1 MeV in the laser produced plasma. Simulation calculations can describe qualitatively the neutron spectra by assuming isotropic deuteron acceleration and a reduction of the reaction probability by a factor of 1/3 for deuterons emitted from the front of the target. These calculations indicate in particular that it is necessary to assume deuterons moving both into and out of the front of the target in order to describe the neutron energy spectra at the two angles. The highest recorded mean neutron yield was about 10^4 neutrons per pulse. The neutron yield increases with the number of electrons emitted from the front of the target and with the intensity of the prompt γ flash induced by the bremsstrahlung of energetic electrons.

DOI: 10.1103/PhysRevE.64.016414 PACS number(s): 52.50.Jm, 52.27.Ny, 52.25.Tx, 29.25.Dz

I. INTRODUCTION

Recent progress in the development of ultraintense lasers enables interesting new laser plasma interaction experiments to be performed. Two types of lasers are used to investigate new phenomena at relativistic intensities.

(i) Large energetic chirped pulse amplification glass laser systems [1–3] deliver single pulses with a duration of 350–500 fs, energies of several tens of joules and, most important, intensities of up to 10^{20} W/cm^2 (even 10^{21} W/cm^2 are envisaged). These energetic ultraintense glass lasers produce electrons and γ rays with energies of up to 100 MeV [4], which give rise to intense ion and proton beams [5–8], high neutron yields from d-D fusion [9–11], photoneutron reactions or nuclear activations [10,12], photonuclear fission [13], as well as extremely high magnetic fields [7,14,15].

(ii) The other type of lasers are the more compact 10-Hz Ti:sapphire lasers with a pulse duration of 30–150 fs, an energy of several hundreds of millijoules, and intensities of up to 10^{19} W/cm^2. These smaller Ti:Sapphire lasers, however, have the advantage of shorter pulse durations, which might be crucial for electron acceleration [16] and higher repetition rates. These rates are important for detailed experiments on short pulse sources of energetic particles like electrons, ions, neutrons, and bremsstrahlung γ rays.

Whereas a relatively large number of papers are devoted to studies of hot electrons, γ rays and, in some cases, ions, studies of femtosecond-laser-pulse-generated neutrons are rare and further detailed investigations are needed. If a solidlike or gaslike target containing deuterium atoms is irradiated by an femtosecond-laser pulse with an intensity of $\geqslant10^{17}$ W/cm^2 it is possible to accelerate deuterons to energies high enough to attain an appreciable cross section for the well-known fusion reaction $d+\mathrm{D}\rightarrow{}^3\mathrm{He}+n+3.269$ MeV. Recent publications demonstrate that neutrons can be produced in solid $(CD_2)_n$ targets [17] as well as in cryogenic D_2-cluster targets [18,19] by compact 10 Hz femtosecond-lasers. Pretzler *et al.* [17] exploited time-of-flight (TOF) techniques to identify and count neutrons from $(CD_2)_n$-plastic targets irradiated by 150-fs pulses of the Ti:sapphire laser, while Ditmire *et al.* [18] reported on neutron counting with energy insensitive BF_3 detectors. An optimum of 10^4 neutrons per laser pulse (120 fs) was observed by investigating the yield as a function of cluster size. Very recently Zweiback *et al.* [19] employed TOF methods for neutron spectrometry.

The investigation of detailed neutron energy spectra is a very interesting topic. The knowledge of such spectra at different angles Ψ_n relative to the incident laser beam and target surface in the case of solid targets carries important information on the momentum vector of accelerated deuterons as well as on the atomic density distribution close to the laser produced plasma. Thus, by measuring the neutron energy $E_n(\Psi_n)$ as well as the double differential neutron yield $d^2Y_n/d\Omega_n dE_n(E_n,\Psi_n)$ one can obtain information on the energy and direction of accelerated deuterons. For illustration, the kinematics and differential cross sections for the reaction D(d,n) are shown in Figs. 1 and 2, respectively, as a function of deuteron energy. The angles Θ_n given in the two figures, however, are relative to the deuteron velocity vector. To establish a relation between Ψ_n and Θ_n is the principal task in the interpretation of the above-mentioned measurements, which, in this way, provide a sensitive tool to probe the ion acceleration in laser produced plasma.

In this work we present a summary and discussion of a recent experimental study of d-D neutron production obtained with a 10-TW Ti:Sapphire laser. Neutron spectra were measured in the direction of the laser beam and approximately perpendicular to it. The energies and directions of the accelerated deuterons will be discussed on the basis of the measured angle dependent neutron energy distributions. In

*Electronic address: hilscher@hmi.de

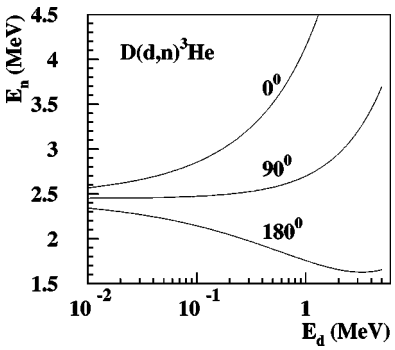

FIG. 1. Kinematical dependence of the neutron energy in the laboratory system at $\Theta_n = 0°$, 90°, and 180° relative to the deuteron velocity as a function of deuteron energy E_d for the reaction $D(d,n)^3He$.

Sec. II we describe the experimental setup. In Sec. III we present the electron and bremsstrahlung yields, which are related to the neutron yield per laser shot. In Sec. IV detailed neutron energy spectra are compared to simulation calculations. The findings are summarized in Sec. V.

II. EXPERIMENT

The investigations were performed with the 10-Hz, 10-TW Ti:Sapphire laser at the MBI. This system produces laser pulses of up to 300 mJ at a central wavelength of 800 nm and with a pulse duration of about 50 fs. For more details of the laser system see Nickles *et al.* [22]. The *p*-polarized beam was focused with a 13-cm dielectric off-axis parabolic mirror onto a thin deuterated plastic target. A 100 μm-thick fused silica plate protected the mirror from target debris. The intensity on target was determined to about 2×10^{18} W/cm^2 by simultaneous measurements of the laser pulse duration, energy, and focal spot size of about 15 μm.

The pulse duration was determined with a second order autocorrelator. Preliminary measurements of the contrast ratio of the 50-fs pulse resulted in a value of about 10^{-4}, which is typical for highly amplifying Ti:Sapphire lasers with a regenerative preamplifier. Therefore targets were exposed to a much longer pulse pedestal preceding the main pulse, which created a small preplasma with a scale length of

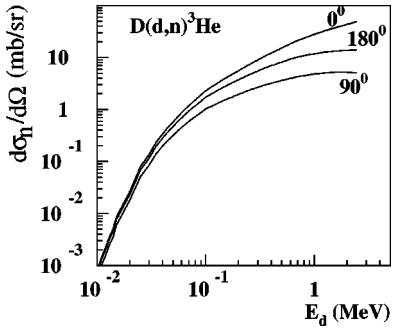

FIG. 2. Neutron cross section in the laboratory system at $\Theta_n = 0°$, 90°, and 180° as a function of the deuteron energy E_d for the reaction $D(d,n)^3He$. The compilations from Refs. [20,21] have been employed.

several laser light wavelengths λ. In addition, the intensity was cross checked by measuring the strong field ionization in Xe atoms under the same irradiation conditions. From the observed maximum ionization stage, Xe^{21+}, an intensity of 2×10^{18} W/cm^2 was estimated using the well-known Amossov-Delone-Krainov formula [23]. This result is consistent with the intensity determination from the pulse length, energy, and spot size.

The target was a 0.2-mm-thick $(CD_2)_n$-plastic layer produced under pressure and heat (about 200 °C) from deuterated polyethylene powder on a 1.8-mm-thick Al disk with a diameter of 4.5 cm. The deuterium was isotopically enriched to 98 at. %. For background measurements, the deuterated polyethylene targets were replaced by polyethylene targets with a natural isotopic hydrogen composition. In order to supply a fresh target area for each laser shot, the target was moved about 200 μm in the target plane (x,y) from shot to shot. The necessary repositioning of the target surface in the direction of the target normal (z) was controlled by a piezosensor in order to keep the target surface in the beam focus with an accuracy of about 1 μm. The angle of incidence of the laser light was 45° relative to the target normal. Each target could be irradiated with about 6000 laser shots at a frequency of 2.5 Hz. The total irradiated target area was 22×26 mm^2.

The produced hot plasma was diagnosed by the following methods: (i) electron TOF measurements [22], (ii) electron counting with and without energy discrimination, (iii) bremsstrahlung intensity measurements, and (iv) TOF neutron spectrometry of the $D(d,n)$ reaction.

Figure 3 shows the setup of the experiment. The magnetic spectrometer MS located at an angle of 157° with the laser beam propagation was equipped with three Si detectors $(M1,M2,M3)$ measuring the number of electrons at mean energies of 160, 620, and 1120 keV for each laser pulse. The single detector Si1 measured the yield of electrons at 82°, irrespective of the energy. The Si diodes were only 40-μm thick and thus were penetrated by most of the electrons. The number of electrons N_{el} per laser pulse was deduced from the ratio of the measured energy per pulse divided by the known energy loss per electron. The energy response of the Si detectors was calibrated with an ^{241}Am α source. The detectors Si1 and MS were positioned inside a vacuum chamber with a diameter of 45 cm and 5-mm-thick stainless steel walls. Al windows with a thickness of 0.5 mm were placed in the direction of the neutron detectors $(N1,N2)$.

Two liquid scintillators (BC501) with a diameter of 25.4 cm and a thickness of 10.2 cm were used as neutron detectors and positioned about 3.8 m from the target at an angle of 112° $(N1)$ and 5° $(N2)$ relative to the incident laser beam. Detector $N1$ was made movable in order to vary the TOF path length, and was shielded by a 15-cm-thick Pb wall placed in front of the scintillator. Detector $N2$ was shielded with 20 cm of Pb. In addition, both detectors were protected by 5 cm of Pb plates on all sides. The intrinsic time resolution of 1 ns full width at half maximum (FWHM) for both detectors was derived from the response of the detectors to prompt γ rays. The resolution for neutrons, however, is considerably larger due to variations of the TOF path length

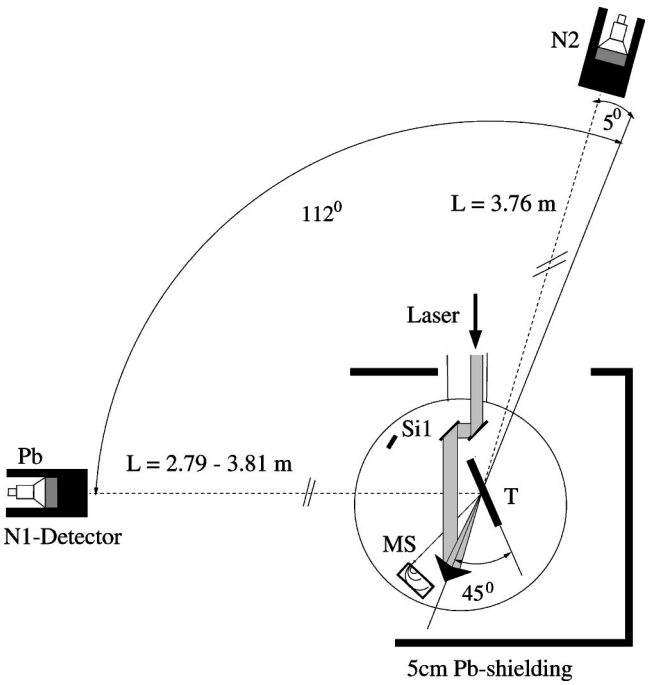

FIG. 3. Experimental setup, T: target, MS: magnetic spectrometer for electrons at $\Psi_{MS}=157°$, Si1: Si detector for integral electron yield measurements at $\Psi_{Si1}=82°$, $N1$ and $N2$: neutron detectors at $\Psi_n=112°$ and 5°. The straight solid line indicates the direction of the incident laser beam axis, all angles are relative to this axis.

over the scintillator thickness and multiple scattering of neutrons in the massive lead shielding [24]. The modification of the TOF signals due to the shielding geometry was simulated with the Monte Carlo code MCNP [25] for neutron, photon, and electron transport. The resulting total time resolution (FWHM) for 1.5 and 3.0 MeV neutrons amounts to 6.8 and 5.8 ns, respectively, corresponding to an energy resolution of 95 and 220 keV. Furthermore, the calculations showed that the broadening of the TOF distribution can be minimized for a given Pb shield in front of the neutron detector by reducing in scattering from the side shielding and by employing a large neutron detection threshold. In the present experiment, the side shielding was 5-cm-thick Pb and the neutron threshold was set at 1 MeV.

For each laser pulse and neutron detector the following four parameters were measured: the energy E_γ of the prompt γ flash recorded by the scintillation detectors, the proton recoil energy E_p related to the detection of a neutron deduced from the charge integrated anode signal, the TOF T_γ of the prompt γ flash, and the delayed neutron TOF T_n. The energy E_γ was determined in two ranges of up to 10 MeV and up to 100 MeV using signals of two different dynodes of the photomultiplier (PM). The low energy channel was calibrated with a ^{22}Na source, while the calibration of the high energy channel was deduced from the energy loss of cosmic muons passing through the scintillator.

The parameter E_γ measures the summed energy of all γ rays as well as the neutrons registered in detector $N1$ or $N2$. The contribution of the neutrons to E_γ is very small, i.e., less than 1 MeV per neutron. The γ rays are produced by bremsstrahlung of energetic electrons in the thick Al backing of the target. More energetic electrons produce γ rays with higher energies that are more strongly focused in the direction of the electrons. Higher γ-ray energies also result in a larger transmission through the massive Pb shielding. Therefore E_γ is correlated with the energy and yield of electrons and consequently also with the magnitude of acceleration fields in the plasma. This interpretation corroborates the finding that E_γ, as recorded by detector $N2$ at 5°, is much larger requiring 5 cm more Pb shielding compared with detector $N1$ at 112°. In this sense we refer to the somewhat complex observable E_γ in the following as the ''yield of energetic γ rays.''

In addition to the four parameters ($E_\gamma, T_\gamma, E_p, T_n$), which were measured for each neutron detector and laser pulse, the number of electrons was recorded in detectors Si1 and MS. A multiparameter data acquisition system made it possible to investigate the correlation of all these measured quantities for each laser shot.

III. ELECTRON AND BREMSSTRAHLUNG YIELD

The coupling of the laser pulse to the plasma mainly depends not only on the pulse energy and the temporal distribution, but also on the target area irradiated, the target parameters, and the irradiation angle of the incident light. The primary coupling process is energy transfer to plasma electrons that can reach values of the order of ~10% [26]. The energetic electrons produce energetic γ rays by bremsstrahlung in the target and the detection of these γ rays can in turn be used to characterize the electron spectrum and yield [26]. These electrons build up electrical fields in the plasma, which accelerate the deuterons responsible for the neutron production. Thus, an analysis of energetic electrons and energetic γ rays should help to identify scalings that will enable us to characterize the plasma particularly suited for neutron production. However, since the experimental irradiation conditions like intensity and pulse shape of the Ti:Sapphire laser could not be varied largely, it was impossible to determine the optimum laser parameters for neutron generation. In a first step, the plasma was characterized by monitoring the total number of electrons at 82°, the number of electrons at different energies at 157°, and additionally the γ rays at the angles of the neutron detectors (5° and 112°).

It is striking to see that the observed quantities have very large shot-to-shot fluctuations, indicating a strong nonlinearity of the coupling of the laser pulse into the plasma most likely caused by variations (not monitored) in the temporal and spatial distribution of the laser pulse. A typical picture of these large shot-to-shot fluctuations of the yield of energetic γ rays E_γ at 112° and the value of the electron number N_{el} at 82° is shown in Fig. 4. Variations of E_γ and N_{el} of up to two and one order of magnitude, respectively, are observed. The corresponding relatively weak correlation of E_γ and N_{el} for about 6000 laser shots is shown in the right top panel of Fig. 4. Similar fluctuations are also observed for the three channels of the magnetic spectrometer, which are, however, strongly correlated. The corresponding distributions of E_γ and N_{el} for 6000 laser shots (including the 1000 shots shown

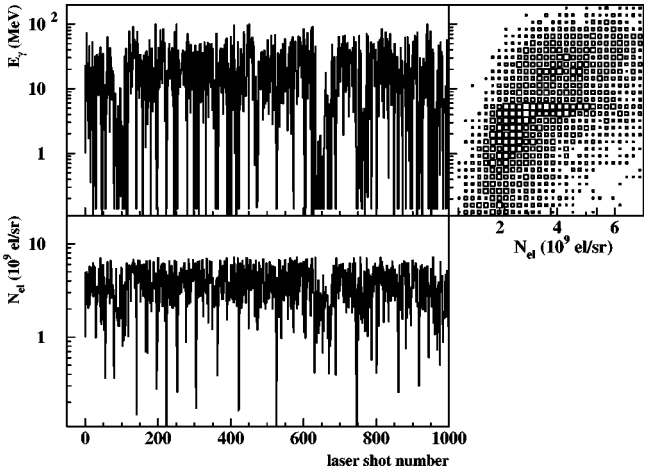

FIG. 4. Shot-to-shot variation of the yield of energetic γ rays as measured with neutron detector $N1$ at 112° and the number of electrons N_{el} measured at 82° for a run with ''good'' coupling. The right top panel displays the two-dimensional correlation of E_γ and N_{el} for all 6000 laser shots.

in Fig. 4) are shown in Fig. 5 for an exceptionally ''good'' run with highly efficient coupling (solid histogram), resulting in the maximum neutron yield as will be shown below, as well as for ''normal'' coupling as for most runs (dashed histogram). The observed discontinuity at $E_\gamma \approx 10$ MeV (also seen in Fig. 4) is an experimental artifact due to switching between two dynodes of the PM in order to change the detection range. Similar shot-to-shot fluctuations have been reported in the literature for the number of accelerated electrons [27], the maximum observed ion energy [8], the ion spectral distribution [28], and the photoneutron activation yield [12]. These fluctuations are most likely caused by variations of the laser pulse, but this subject needs further investigation.

One can conclude from these experimental results that both the yield of energetic γ rays E_γ as well as the number of electrons N_{el} are sensitive to the coupling of the laser pulse to the plasma. The higher sensitivity of the yield of

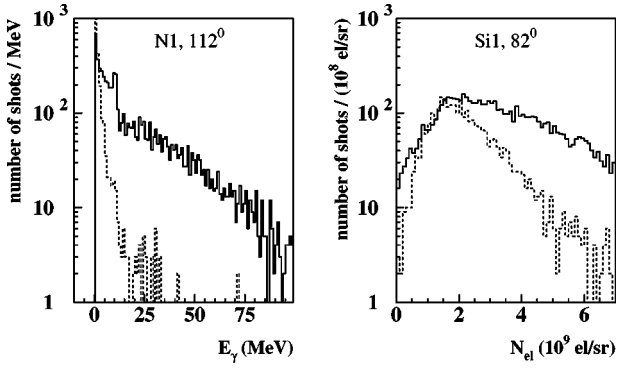

FIG. 5. Number of laser shots as a function of the yield of energetic γ rays E_γ measured at 112° and the integral number of electrons N_{el} at 82° for two runs with ''good'' (solid histogram) and ''normal'' (dashed histogram) coupling. The corresponding mean values are 19.1 (2.8) MeV and 3.21 (2.26)$\times 10^9$ electrons/sr for E_γ and N_{el}, respectively.

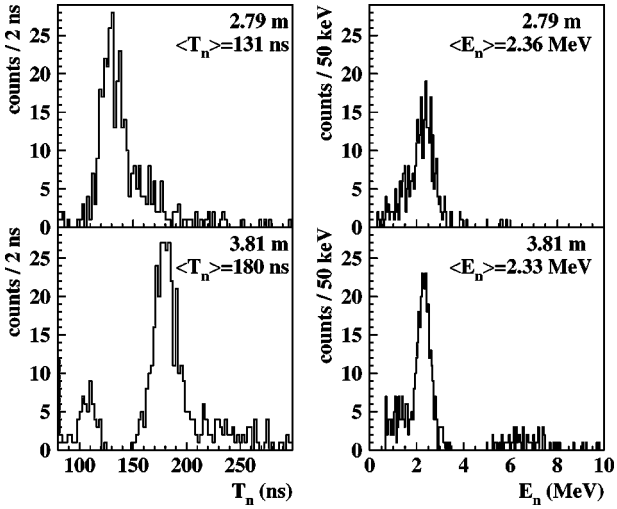

FIG. 6. Neutron TOF and energy spectra measured at 112° with two different path lengths of 2.79 and 3.81 m. Note the suppressed zero of the TOF axis T_n.

energetic γ rays is due to the fact that this observable is more strongly correlated (Sec. II) with the production of energetic electrons and therefore with higher acceleration fields. Both signals were used to monitor the plasma production during the experimental campaign. In the following we report on the neutron yield as a function of these observables.

IV. NEUTRON SPECTRA AND NEUTRON YIELD

The left two panels of Fig. 6 show the neutron TOF spectra that were measured with detector $N1$ (112°) at distances of 2.79 and 3.81 m. The position of the prominent peak in these spectra scales very closely with the flight path and consequently both spectra, when converted to neutron energy (right panels), show the peak at approximately the same energy, 2.36 or 2.33 MeV, respectively. The tails to longer TOF or lower energy are most likely due to neutrons scattered in the Pb shielding. The spurious peak at about 100 ns or 6 MeV will be discussed below.

In spite of the massive lead shielding the huge prompt γ flash produced in the target induces large signals (E_γ) in the neutron detectors. These large signals cause a dead time during which retriggering by delayed signals such as neutrons is suppressed. This is shown in the top panels of Fig. 7 where no events occur in the top left regions of the two-dimensional spectra of E_γ vs T_n for deuterated and nondeuterated targets. This demonstrates the need for choosing the TOF path lengths long enough so that the neutron flight time T_n to be measured is larger than the detector dead time that depends on E_γ and thus also on the laser coupling. Alternatively, more lead shielding could be used but then the time resolution for neutrons would decrease.

Projections of the two-dimensional spectra are shown in the middle panels of Fig. 7. In addition to the d-D neutrons between $T_n = 150$ and 230 ns or 1.5 and 3.5 MeV, indicated by the gray shaded area in the left panel, two spurious TOF peaks are observed at about 105 and 270 ns. The peak at 270 ns is due to reflections of very large anode pulses whereas

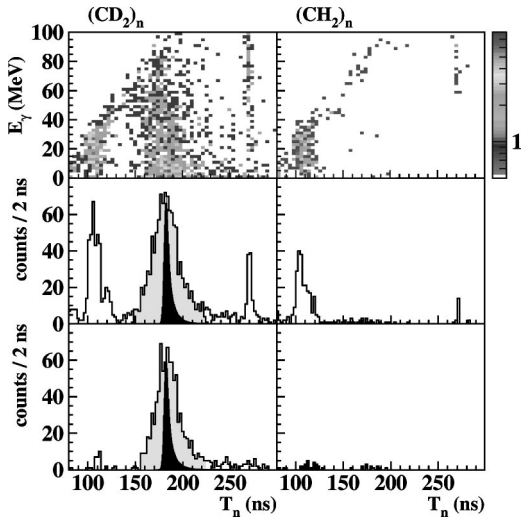

FIG. 7. Top panels: Two-dimensional plot of the yield of energetic γ rays E_γ as measured with the neutron detector at 112° versus neutron TOF T_n for a $(CD_2)_n$ (left panels) and $(CH_2)_n$ (right panels) target. Middle panels: Projection on the TOF axis; the TOF region corresponding to neutron energies between 1.5 and 3.5 MeV are indicated by the shaded area. Bottom panels: same as middle panels but with the recoil condition. Note the suppressed zero of the TOF axis T_n in all panels. The experimental time resolution for monoenergetic (2.3 MeV) neutrons is indicated by the narrow black histogram.

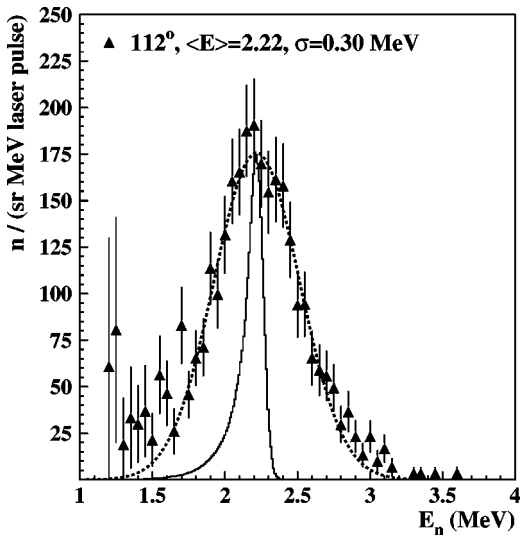

FIG. 8. Double differential neutron yield $d^2Y_n/d\Omega_n dE_n(E_n,\Psi_n)$ at $\Psi_n=112°$ for a run with good laser coupling with the largest observed neutron production, see also Figs. 5 and 9. The dashed line is a Gaussian fit to the data, the mean energy $\langle E\rangle$ and the standard deviation σ are given. The histogram indicates the calculated energy resolution.

the origin of the peak at 105 ns is not fully understood. The black narrow peaks shown in the time-of-flight distributions of Fig. 7 reflect the calculated time resolution for monoenergetic neutrons of 2.3 MeV as described in Sec. II.

We have also measured the charge integrated anode signal at the time T_n corresponding to the proton recoil energy E_p from neutron scattering off hydrogen in the organic scintillator. Therefore we can analyze the TOF under the condition that the energy E_n, as deduced from TOF, fulfills the condition: $E_p < fE_n$. The factor f was chosen to be 2 instead of 1 in order not to reject pileup events when two neutrons from the same laser pulse are registered. The probability of such pileup events can be up to 25% for the largest neutron yield with about 0.5 neutrons detected per laser shot. The TOF spectrum sorted with this recoil condition is shown in the lower left panel of Fig. 7. The shaded region corresponding to d-D neutrons is essentially unchanged while both spurious peaks have almost completely disappeared.

To further test that the observed neutrons are due to the d-D reaction, measurements were carried out with nondeuterated polyethylene targets under the same experimental conditions. The corresponding spectra are shown in the three right panels of Fig. 7 accumulated for the same number of laser shots as in the left panels. The few counts observed in the TOF interval of 150 to 220 ns (or 1.5 to 3.5 MeV) correspond to a background of less than 1%.

In the following we describe the measured energy spectra of neutrons from the $D(d,n)$ reaction. Figure 8 shows the TOF spectrum of Fig. 7 (left panel) after transformation to neutron energy. The neutron yield has been corrected for the energy dependent detection efficiency as calculated with the Cecil *et al.* code [29] as well as for absorption and out scattering in the 15-cm Pb shield. The Pb correction of about 1/0.51 has been deduced from a calibration measurement in a similar geometry with neutrons from a ^{252}Cf source with mean energies of 2.1 MeV in coincidence with fission fragments resulting in a transmission of about 80% through 5 cm of Pb. The out scattering and absorption of neutrons in the lead shielding, which is different for $N1$ and $N2$, represent the major uncertainty of about 25% in the relative neutron yield from the two detectors. The dashed line in Fig. 8 corresponds to a Gaussian fit giving a mean energy of 2.22 MeV and a standard deviation of 0.30 MeV. We observe that the mean energy is smaller than the neutron energy of 2.45 MeV at the threshold of the $D(d,n)$ reaction. This indicates that at the detection angle of 112°, the neutrons are emitted at least partially in the direction opposite to that of the deuterons (see Fig. 1). In addition, a very large width for the experimental energy distribution of about 700 keV (FWHM) is observed, which is much larger than the experimental energy resolution as indicated in Fig. 8 by the histogram for monoenergetic (2.3 MeV) neutrons.

Before describing these results further we will briefly discuss correlations of the total neutron yield per laser shot with the number of electrons N_{el} and the yield of energetic γ rays E_γ (as defined in Sec. II). For this purpose the neutron yield was integrated between energies of 1.5 and 3.5 MeV and over 4π sr assuming isotropic neutron emission. Figure 9 shows for a ''good'' run (solid line in Fig. 5) the correlation of the total neutron yield per laser shot with E_γ detected at $\Psi_n=112°$ (left panel) and N_{el} at 82° (right panel). We cannot show the corresponding correlation for neutron detector $N2$ since this detector was not operating correctly during this run with a highly efficient laser coupling. Although an increase of the total neutron yield with both the electron and

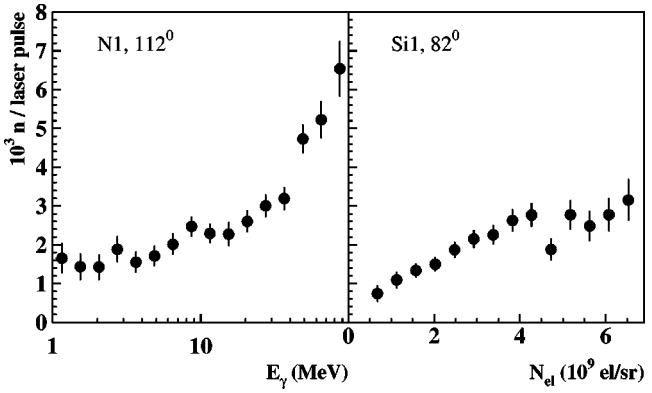

FIG. 9. Number of neutrons emitted per laser pulse as a function of E_γ for neutron detector $N1$ at 112° (left panel) and as a function of the number of electrons detected at 82° (right panel).

the γ signal is observed, it is obvious that the neutron yield scales much more strongly with E_γ. An increase from about 1500 neutrons per laser shot at $E_\gamma \approx 1$ MeV up to 6500 neutrons at $E_\gamma \approx 100$ MeV is observed. Recalling the definition of E_γ as the summed energy of γ rays and neutrons we note that the energy E_γ of about 1 MeV already corresponds to the maximum recoil energy deposited in the scintillator by a 3-MeV neutron. Consequently the low neutron yield of about 1500 neutrons per shot is associated with few or no γ rays detectable behind a 15-cm-thick Pb shield. A similar weak correlation between the neutron yield and N_{el} from Si1 was also observed for the electron signals recorded in the three channels of the magnetic spectrometer as shown in Fig. 10.

In summary, we note that the neutron yield is more strongly correlated with the γ-ray yield than with the number of electrons emitted from the target. The strong correlation with E_γ can be understood by recalling that E_γ is a sensitive monitor of energetic electrons (Sec. II). These energetic electrons are responsible for higher electric fields, which in turn can accelerate the deuterons more efficiently, resulting in a larger neutron production. The weak correlation between neutron yield and N_{el}, on the other hand, may be due to the fact that both electron detectors (MS and Si1) were positioned at angles of 23° and 53° relative to the target normal. Consequently, both detectors only record electrons emitted from the front of the target, while more energetic electrons

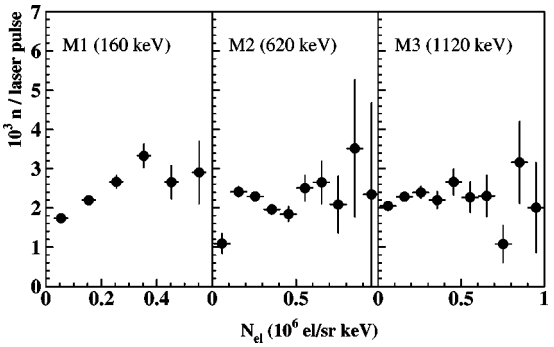

FIG. 10. Number of neutrons emitted per laser pulse as a function of the number of electrons N_{el} detected in the three channels $M1$,$M2$, and $M3$ of the magnetic spectrometer at 157°.

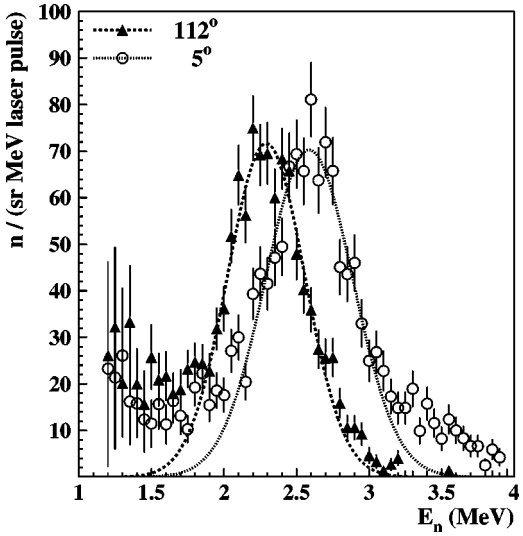

FIG. 11. Neutron energy spectra (triangles and circles) measured simultaneously at 112° and 5° and Gaussian fits (dashed and dotted lines) to the data points with mean energies $\langle E \rangle$ (standard deviation σ) of 2.29 (0.27) and 2.59 (0.30) MeV, respectively.

have a higher probability to be directed into the target [10,12]. The detection of electron emission from the rear of the target was not possible in the present experiment owing to the 1.8-mm-thick Al backing of the target.

As pointed out in the Introduction, details of the double differential neutron energy spectra provide important information on the energy and direction of accelerated deuterons and therefore also indirectly on electric fields induced in the plasma and target. In order to illustrate this, Fig. 11 shows two neutron energy spectra measured simultaneously at $\Psi_n = 5°$ and 112° relative to the laser beam with ''normal'' coupling. The error bars include counting statistics and the systematic uncertainty of the neutron detection efficiency that causes particularly large error bars close to the neutron detection threshold of 1.0 MeV. Neither the uncertainty of about 25% for the relative yield due to different amounts of Pb shielding in front of $N1$ (15 cm) and $N2$ (20 cm), nor the systematic absolute error due to neutron absorption and out scattering in the lead shielding are included in the error bars.

First it is interesting to note that the neutron spectra at 112° measured with ''good'' (Fig. 8) and ''normal'' (Fig. 11) laser coupling show a very similar spectral shape (width and mean energy) while the maximum double differential yield is about three times smaller in the latter case. Comparing the two simultaneously measured neutron energy spectra of Fig. 11 we note that they are shifted relative to each other by about 300 keV and that the high energy tail of the spectrum at 5° extends up to about 4 MeV requiring deuterons of energies of up to about 1 MeV for forward neutron emission (see Fig. 1).

The dotted and dashed curves in Fig. 11 are Gaussian fits to the spectra measured at 5° and 112°, respectively. From these fits we deduce mean neutron energies of 2.29 MeV at 112° and 2.59 MeV at 5°. These energies are below and above 2.45 MeV, the energy one would expect for neutron emission at 90° relative to the deuteron velocity vector for

deuteron energies up to about 100–200 keV, as shown in Fig. 1. From this finding we can conclude qualitatively that (i) either the deuterons are preferentially accelerated into one direction or the density distribution of deuterium atoms in or close to the plasma induces a forward-backward asymmetry, and (ii) this direction differs from the direction of the incident laser beam. More precisely, one finds that the two mean neutron energies as measured by the almost orthogonally positioned neutron detectors are consistent with deuterons being accelerated to about 30 keV into the target at an angle of about 40° relative to the laser beam. It is worth noting here that acceleration of protons and ions in the direction perpendicular to the target surface was previously observed [5,7,12], but for remarkably higher intensities (about 5×10^{19} W/cm^2) than in the present case.

From the qualitative findings (i) and (ii) one would expect, however, to record two very narrow neutron lines at 2.29 and 2.60 MeV with a width given essentially by the experimental energy resolution of 140 and 180 keV, respectively. Whereas the two peak energies agree with the experiment, the widths disagree and are about 700 keV (FWHM). The large widths of the measured energy distributions indicate large variations of the deuteron velocities in magnitude as well as in direction. Such variations should be expected considering the large fluctuations of the coupling of the laser pulse into the plasma (see Fig. 4) described in Sec. III. More detailed studies of the dependence of the neutron energy spectra for different ranges of E_γ and N_{el} would be very interesting, but in the present experiment the accumulated statistics were not sufficient to perform such an analysis.

To exploit these findings in greater detail we performed a simple Monte Carlo (MC) simulation by assuming that the deuterons are accelerated isotropically in all directions. The experimental result of forward-backward asymmetry is modeled by assuming that deuterons with velocity vectors pointing into the target have a larger probability (P_{in}) to initiate a D(d,n) reaction than those moving out of the target (P_{out}) with $P_{out}=f_\rho\times P_{in}$ and $f_\rho<1$. The factor f_ρ was used as a free parameter and might be interpreted as a reduction of the deuterium atom density in front of the target surface seen by deuterons accelerated into the hemisphere extending from the target surface into the vacuum. The reaction probability $P_{reac}(E_d,\Theta_n)$ that deuterons of energy E_d between 0.01 and 1.0 MeV initiate a D(d,n) reaction with neutron emission at an angle Θ_n relative to the deuteron velocity vector was assumed to be given by the relation $P_{reac}(E_d,\Theta_n)\sim\sigma(E_d,\Theta_n)/E_d^2$. The cross sections $\sigma(E_d,\Theta_n)$ were calculated according to Refs. [20,21]. The $1/E_d^2$ distribution is introduced tentatively in order to describe for increasing E_d both the decrease of the probability to accelerate deuterons and the increase of their range resulting in larger reaction probabilities. The broadening of the TOF distributions due to multiple scattering in 15 and 20 cm of Pb shielding is taken into account by exploiting MCNP calculations (see Sec. II) for ten neutron energies between 1.75 and 4.00 MeV.

The result of this MC simulation for $f_\rho=0.3$ is represented by the solid curves in Fig. 12. The absolute yield is normalized arbitrarily but with the same normalization factor for 112° and 5°. We observe that the measured neutron energy distribution is approximately reproduced by the simulation. Even the high energy tails at 5° are described reasonably well.

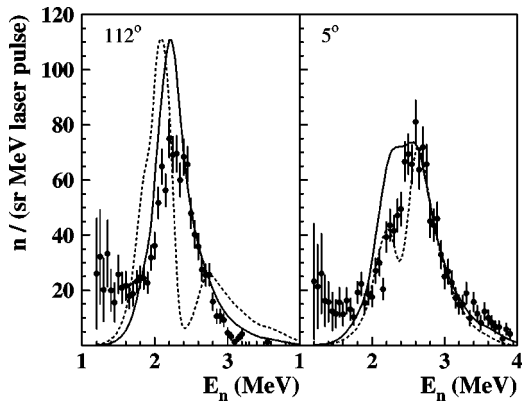

FIG. 12. Neutron energy spectra measured simultaneously at 112° (left panel) and 5° (right panel). The solid and dashed curves represent the result of MC simulations (see text) assuming an isotropic angular distribution of deuterons and emission into two cones with half opening angles of 22.5°, respectively.

The assumption of an isotropic ion emission is not consistent with the recently reported [7,8] angular distributions of energetic protons and other ions from experiments with ultrahigh intensity ($I\approx5\times10^{19}$ W/cm^2) laser interactions on thin Al targets. Krushelnick *et al.* [7] observed the emission of protons with energies between 2.8 and 20 MeV into narrow cones from the front and rear of the target foils. With decreasing proton energy the half-angle of the cones increases to about 30° at the lowest proton energy of 2.8–4 MeV. For comparison with those results we show in Fig. 12 (dashed line) a simulation assuming a cone half-angle of 22.5° instead of isotropic emission with otherwise no changes. The symmetry axis is chosen parallel to the target normal. We observe two separate peaks with high and low neutron yield corresponding to deuterons moving into and out of the target surface, respectively. Though the measured neutron energy spectra are less well described we learn from the spectra shown (dashed line) that one has to assume that deuterons are also accelerated out of the target. Without this assumption it is not possible to describe simultaneously at 112° the high energy component of the neutron spectrum above about 2.4 MeV on one hand and at 5° the low energy part below about 2.4 MeV on the other. By increasing the cone half-angle to 90° one can achieve filling the observed minima around 2.4 MeV.

The reason that considerably larger opening angles are needed to describe the measured neutron energy spectra in the present experiment at remarkably lower laser intensities might be due to (i) smaller deuteron energies and (ii) the presence of large magnetic fields that will bend, as suggested by Krushelnick *et al.* [7], the ion trajectories along which the D(d,n) reaction can be initiated. In this context it should be noted that there is an essential difference between the direct observation of ions and their detection by means of an ion-induced nuclear reaction. The latter measures the reaction probability or absorption along the ion trajectories in the plasma region and surrounding target material while the

former measures essentially the transmission through that region. Since the laser intensity in the present case was about one order of magnitude smaller than the one employed by Krushelnick and co-workers [7,8], this comparison should be treated with some caution.

Contrary to the above-discussed observation of narrow emission cones [7,8] Pretzler *et al.* [17] have suggested radial acceleration along the laser plasma channel due to Coulomb explosion, which was also experimentally observed in underdense plasma [6]. It is worth noting that in the present experiment the effect of a radial acceleration of ions could also partially appear. This follows from the experimental fact that the laser pulse contrast was poor, resulting in a relatively long plasma density gradient length (several λ) so that self-focusing of the laser pulse could occur. A beam breaking into self-focusing channels can result in an undercritical plasma at laser powers $P > P_{cr} \simeq 17$ GW $(\omega/\omega_p)^2$, where ω is the laser frequency and ω_p is the plasma frequency. Assuming that in the present case $\omega \sim \omega_p$, the intensity in the focused beam is $I \sim 2 \times 10^{18}$ W/cm^2, and the laser spot diameter $2w$ is smaller than 15 μm, one arrives at a laser power of $P \simeq 3.6$ TW, which fulfills in principle the conditions for self-focusing. Therefore a superposition of the effects of axial and radial accelerations alternating from shot to shot could well be the reason for the finding that the isotropy assumption best describes the measured spectra. Further investigations with laser pulses of controlled intensity and pulse shape are needed to determine the dominant acceleration processes.

In summary, it is possible to describe the two main characteristics of the experimental neutron energy distributions, (i) the large width of about 700 keV (FWHM) and (ii) the energy shift of about 300 keV at two detection angles differing by 107°. The empirically found parameters of the simulation indicate that deuterons are accelerated up to 1 MeV and the angular distribution of deuterons initiating a (d,n) reaction is nearly isotropic. Furthermore, the target surface defines an asymmetry: either about 30% of the deuterons move out of the front of the target, as compared to those moving towards the rear, or they have a smaller probability to initiate a reaction owing to a reduced deuterium atom density. There remain, however, open questions: how unique are the assumptions and in particular, what is the influence of fluctuations in the coupling of the laser pulse to the plasma. The observed large fluctuations of this coupling could give rise to completely different plasma regimes resulting in different acceleration fields. It will be a challenge for future experiments to produce a well-defined plasma and to investigate the deuteron acceleration by measuring detailed neutron energy spectra in a wide angular range. Well-defined plasmas are in particular also needed for the comparison with three-dimensional theoretical particle-in-cell calculations. Detailed numerical calculations are in progress and will be published in a separate paper.

V. CONCLUSIONS

We have carried out detailed investigations of the neutron energy spectra from the D(d,n) reaction induced by the interaction of 50-fs laser pulses at intensities of about 2×10^{18} W/cm^2 and a repetition rate of 2.5 Hz in solid $(CD_2)_n$ targets. The maximum obtained mean neutron yield was about 10^4 neutrons per pulse indicating that a femtosecond Ti:sapphire laser driven D(d,n) reaction should be a very promising neutron source after further enhancement of the total neutron number.

The most important property of the neutron energy spectra measured at two angles (5° and 112°) is the very large width of 700 keV (FWHM) and the energy shift of about 300 keV between the peak positions corresponding to the two detection angles. The maximum measured neutron energy of about 4 MeV indicates that deuterons are accelerated up to about 1 MeV. Furthermore, the large widths in the neutron spectra also point to large variations of the deuteron velocities in magnitude and direction.

The experimental neutron energy distributions can be reproduced qualitatively by a simulation assuming isotropic deuteron acceleration and a reaction probability reduced to about 30% for deuterons moving out of the front of the solid $(CD_2)_n$ target. The latter assumption can be interpreted either as a reduction of the deuterium atom density seen by deuterons being accelerated out of the target or a smaller probability for acceleration in this direction. Such an ambiguity could not be resolved experimentally in the present experiment since the measured reaction probability is given by the product of the number of accelerated deuterons and the number of target atoms within the deuteron range. The simulations clearly indicate that deuterons are accelerated both into and out of the front of the target.

It has been shown that the mean neutron yield per pulse strongly increases with the yield of energetic γ rays produced by more energetic electrons and less steeply so with the number of electrons emitted from the front surface of the solid target at 82° and 157° relative to the laser beam.

Large pulse-to-pulse fluctuations of the number of electrons and the γ-ray intensity are caused most likely by variations of the laser pulse and indicate a strong nonlinearity in the coupling of the laser pulse to the plasma. These strong variations may give rise to different plasma regimes and hence acceleration fields that vary in magnitude and direction, resulting in the experimentally observed large widths of the neutron energy distributions.

ACKNOWLEDGMENTS

We would like to thank the MBI Ti:Sapphire laser crew for the preparation and operation of the laser. The work was supported by the Deutsche Forschungsgemeinschaft Project No. BE 784/6-1,2.

[1] M. Perry, Sci. Technol. Rev. **12**, 4 (1996); Report No. UCRL-52000 (unpublished).

[2] C.N. Danson, J. Collier, D. Neely, L.J. Barzanti, A. Damerell, C.B. Edwards, M.H.R. Hutchinson, M.H. Key, P.A. Norreys, D.A. Peppler, I.N. Ross, P.F. Taday, W.T. Toner, M. Trentelman, F.N. Walsh, T.B. Winstone, and R.W.W. Wyatt, J. Mod. Opt. **45**, 1653 (1998).

[3] C. Rouyer, N. Blanchot, I. Allais, E. Mazataud, J.L. Miquel, M. Nail, A. Pierre, C. Sauteret, and A. Migus, J. Opt. Soc. Am. B **13**, 55 (1996).

[4] D. Gordon, K.C. Tzeng, C.E. Clayton, A.E. Dangor, V. Malka, K.A. Marsh, A. Modena, W.B. Mori, P. Muggli, Z. Najmudin, D. Neely, C. Danson, and C. Joshi, Phys. Rev. Lett. **80**, 2133 (1998).

[5] S.P. Hatchett, C.G. Brown, T.E. Cowan, E.A. Henry, J.S. Johnson, M.H. Key, J.A. Koch, A.B. Langdon, B.F. Lasinski, R.W. Lee, A.J. Mackinnon, D.M. Pennington, M.D. Perry, T.W. Phillips, M. Roth, T.C. Sangster, M.S. Singh, R.A. Snavely, M.A. Stoyer, S.C. Wilks, and K. Yasuike, Phys. Plasmas **7**, 2076 (2000).

[6] K. Krushelnick, E.L. Clark, Z. Najmudin, M. Salvati, M.I.K. Santala, M. Tatarakis, A.E. Dangor, V. Malka, D. Neely, R. Allott, and C. Danson, Phys. Rev. Lett. **83**, 737 (1999).

[7] K. Krushelnick, E.L. Clark, M. Zepf, J.R. Davies, F.N. Beg, A. Machacek, M.I.K. Santala, M. Tatarakis, I. Watts, P.A. Norreys, and A.E. Dangor, Phys. Plasmas **7**, 2055 (2000).

[8] E.L Clark, K. Krushelnick, M. Zepf, F.N. Beg, M. Tatarakis, A. Machacek, M.I.K. Santala, I. Watts, P.A. Norreys, and A.E. Dangor, Phys. Rev. Lett. **85**, 1654 (2000).

[9] P.A. Norreys, A.P. Fews, F.N. Beg, A.R. Bell, A.E. Dangor, P. Lee, M.B. Nelson, H. Schmidt, M. Tatarakis, and M.D. Cable, Plasma Phys. Controlled Fusion **40**, 175 (1998).

[10] M.H. Key, M.D. Cable, T.E. Cowan, K.G. Estabrook, B.A. Hammel, S.P. Hatchett, E.A. Henry, D.E. Hinkel, J.D. Kilkenny, J.A. Koch, W.L. Kruer, A.B. Langdon, B.F. Lasinski, R.W. Lee, B.J. MacGowan, A. MacKinnon, J.D. Moody, M.J. Moran, A.A. Offenberger, D.M. Pennington, M.D. Perry, T.J. Phillips, T.C. Sangster, M.S. Singh, M.A. Stoyer, M. Tabak, G.L. Tietbohl, M. Tsukamoto, K. Wharton, and S.C. Wilks, Phys. Plasmas **5**, 1966 (1998).

[11] L. Disdier, J-P. Garconnet, G. Malka, and J-L. Miquel, Phys. Rev. Lett. **82**, 1454 (1999).

[12] M.I.K. Santala, M. Zepf, I. Watts, F.N. Beg, E. Clark, M. Tatarakis, K. Krushelnick, A.E. Dangor, T. McCanny, I. Spencer, R.P. Singhal, K.W.D. Ledingham, S.C. Wilks, A.C. Machacek, J.S. Wark, R. Allott, R.J. Clarke, and P.A. Norreys, Phys. Rev. Lett. **84**, 1459 (2000).

[13] T.E. Cowan, A.W. Hunt, T.W. Phillips, S.C. Wilks, M.D. Perry, C. Brown, W. Fountain, S. Hatchett, J. Johnson, M.H. Key, T. Parnell, D.M. Pennington, R.A. Snavely, and Y. Takahashi, Phys. Rev. Lett. **84**, 903 (2000).

[14] E.L. Clark, K. Krushelnick, J.R. Davies, M. Zepf, M. Tatarakis, F.N. Beg, A. Machacek, P.A. Norreys, M.I.K. Santala, I. Watts, and A.E. Dangor, Phys. Rev. Lett. **84**, 670 (2000).

[15] M. Borghesi, A.J. MacKinnon, A.R. Bell, R. Gaillard, and O. Willi, Phys. Rev. Lett. **81**, 112 (1998).

[16] E. Esarey and P. Sprangle, IEEE Trans. Plasma Sci. **24**, 252 (1996).

[17] G. Pretzler, A. Saemann, A. Pukhov, D. Rudolph, T. Schätz, U. Schramm, P. Thirolf, D. Habs, K. Eidmann, G.D. Tsakiris, J. Meyer-ter-Vehn, and K.J. Witte, Phys. Rev. E **58**, 1165 (1998).

[18] T. Ditmire, J. Zweiback, V.P. Yanovsky, T.E. Cowan, G. Hays, and K.B. Wharton, Phys. Plasmas **7**, 1993 (2000).

[19] J. Zweiback, T.E. Cowan, R.A. Smith, J.H. Hartley, R. Howell, C.A. Steinke, G. Hays, K.B. Wharton, J.K. Crane, and T. Ditmire, Phys. Rev. Lett. **85**, 3640 (2000).

[20] H. Liskien and A. Paulsen, Nucl. Data Tables **11**, 569 (1973).

[21] A. Boughrara, H. Beaumevieille, and S. Ouichaoui, Europhys. Lett. **48**, 264 (1999).

[22] P.V. Nickles, M.P. Kalachnikov, P.J. Warwick, K.A. Janulewicz, W. Sandner, U. Jahnke, D. Hilscher, M. Schnürer, R. Nolte, and A. Rousse, Quantum Electron. **29**, 444 (1999).

[23] M.V. Amossov, N.B. Delone, and V.P. Krainov, Zh. Éksp. Teor. Fiz. **91**, 2008 (1986) [Sov. Phys. JETP **64**, 1191 (1986)].

[24] R.J. Leeper and J. Chang, IEEE Trans. Nucl. Sci. **NS-29**, 798 (1982).

[25] Los Alamos National Laboratory Report No. LA-12625-M, 1997 (unpublished).

[26] M. Schnürer, R. Nolte, A. Rousse, G. Grillon, G. Cheriaux, M.P. Kalachnikov, P.V. Nickles, and W. Sandner, Phys. Rev. E **61**, 4394 (2000).

[27] A. Ting, C.I. Moore, K. Krushelnick, C. Manka, E. Esarey, P. Sprangle, R. Hubbard, H.R. Burris, R. Fischer, and M. Baine, Phys. Plasmas **4**, 1889 (1997).

[28] A.P. Fews, P.A. Norreys, F.N. Beg, A.R. Bell, A.E. Dangor, C.N. Danson, P. Lee, and S.J. Rose, Phys. Rev. Lett. **73**, 1801 (1994).

[29] R.A. Cecil, B.D. Anderson, and R. Madey, Nucl. Instrum. Methods **161**, 439 (1979).